Design and performance study of a dielectric-filled cavity beam current monitor for HUST-PTF*

Jiqing Li,[1] Kuanjun Fan,[1,†] Zhengzheng Liu,[1] Jian Wang,[1] Qushan Chen,[1] and Jinfeng Yang[2]

[1]*State Key Laboratory of Advanced Electromagnetic Engineering and Technology, School of Electrical and Electronic Engineering, Huazhong University of Science and Technology, Wuhan 430074, China*

[2]*The Institute of Scientific and Industrial Research, Osaka University, 8-1 Mihogaoka, Ibaraki, Osaka 567-0047, Japan*

To guarantee the exact proton dose applied to patients and ensure treatment safety while disrupting and destroying tumor cells, it is essential to accurately monitor the proton beam current in real-time during patient treatment. Because clinical treatment requires a proton beam current in the ∼nA range, nondestructive beam current monitors (BCMs) are preferred to minimize the degradation of beam quality. However, this poses significant challenges in accurately monitoring such extremely low beam intensities. This study proposes a cavity-type BCM equipped with a dielectric plate to reduce its dimensions and achieve sufficient measurement sensitivity for practical requirements. A prototype cavity BCM was fabricated, and offline testing was performed using a metal wire to simulate the beam to study its performance. Both the simulation and experimental results showed that the cavity BCM could measure ultralow proton beam currents with a resolution up to 0.03 nA.

Keywords: proton therapy; beam current; cavity BCM; nondestructive

1. Introduction

Proton therapy has the obvious advantage of improving clinical outcomes over traditional radiation therapies owing to the Bragg peak of the proton dose distribution [1]. The proton therapy facility HUST-PTF is currently being developed at Huazhong University of Science and Technology. Fig. 1 shows the facility layout, consisting of a 250-MeV superconducting cyclotron, a beam transport line, two rotating gantries, and a fixed treatment room [2].

A synchrotron-based proton therapy facility can adjust the output energy to match clinical requirements, and the beam current can remain relatively constant at different energies. In contrast, a cyclotron-based proton therapy facility requires an energy selection system (ESS) to modulate the fixed-beam energy to kill tumor cells at different depths. The ESS for HUST-PTF consists of a degrader, a set of collimators, and an achromatic system. The stopping materials reduce the proton beam energy from 250 to 70-230 MeV to meet clinical requirements. However, protons undergo severe multiple scattering when they penetrate the stopping materials and lose energy. The proton beam divergence and beam energy spread increase significantly, and only a small portion of the proton beam can be selected by the ESS, resulting in a low and energy-dependent beam transmission efficiency. The lower the required clinical beam energy, the thicker the degrader that protons need to penetrate, and the more severe the scattering effects experienced by protons, the worse the beam quality, leading to a lower transmission efficiency.

When the clinical beam energy changes from 70 to 230 MeV, the transmission efficiency varies from 0.07 to 8.34% for a fixed beam energy of 250 MeV and a carbon degrader material. Suppose the extraction beam current of the cyclotron is 500 nA. The resulting beam current would have a very broad dynamic range of 0.35–41.7 nA, which poses significant challenges for the beam current monitor (BCM) system. Furthermore, this creates difficulties in exactly controlling the treatment dose in practical applications. Therefore, the dynamic range of the proton beam current after passing through the ESS must be confined. In practice, we can adjust the beam current inside the cyclotron and select different collimators to minimize the dynamic range of the clinical proton beam current. We propose that the cyclotron works in three modes that can provide the proton beam intensity at three fixed values, 500 nA, 200 nA, and 60 nA, to compensate for the energy-dependent transmission efficiency. Consequently, depending on the output beam energy, the beam current will decrease from 500 to 0.35–5 nA before and after the ESS. The detailed beam parameters at the extraction of the cyclotron and after the ESS are listed in Table 1.

Table 1. Beam parameters at the extraction of the cyclotron and after the energy selection system.

Beam properties	Units
Extracted beam current	$\leq$ 500 nA
Momentum spread at extraction	0.5%
Beam current beyond the ESS	0.35–5 nA
Momentum spread at the ESS exit	0.5%
Bunch length at the ESS exit for all energies	200 mm
Repetition rate	73 MHz

Monitoring and accurate control of online clinical beam currents are mandatory to guarantee treatment safety. Although traditional ionization chambers can precisely measure the online beam current, they can cause several harmful effects, such as beam scattering and detector activation. Noninvasive BCMs are preferable for minimizing interference with the clinical proton beam, particularly in cases of very low beam intensity. Conventional nondestructive BCMs typically detect the induced electromagnetic fields or image currents. For example, signal pick-ups of the button-type or stripline-type are employed to detect the beam current; however, the output signals are relatively weak and beam position-dependent, containing significant thermal noise owing to their

* This work was supported by the National Natural Science Foundation of China (No.12235005) and the National Key Research and Development Program of China (No. 2016YFC0105309).

† Corresponding author, kjfan@hust.edu.cn

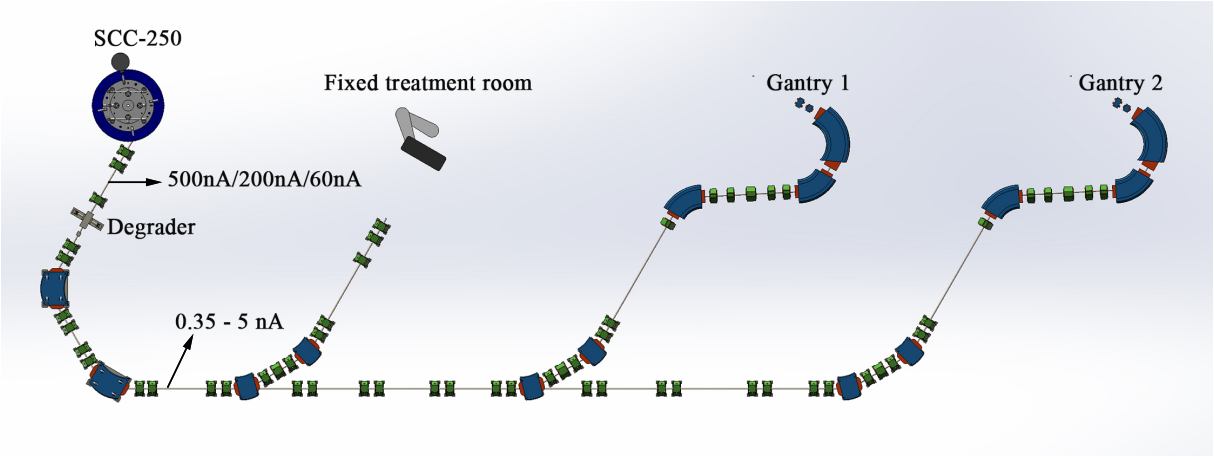

Fig. 1. General layout of HUST-PTF.

broadband basis [3]. Other noninvasive BCMs, such as wall current monitors and fast current transformers, are not suitable for HUST-PTF because their detection threshold cannot be reduced to an average beam current of 1 nA [4].

Cavity-type beam monitors, which detect only a single harmonic of the beam spectrum, have superior current and position detection resolutions. They can generate sufficiently induced signals, even with an average beam current of 1 nA and have negligible effects on the passing beam itself [5]. Usually, two cavity working modes are employed: the monopole mode (TM010) for beam current measurement, and the dipole mode (TM110) for beam position diagnostics [6,7]. Compared with broadband monitors, cavity monitors output signals in a narrowband at the resonant frequency, which significantly reduces the thermal noise. In recent years, the cavity monitors used in medical accelerators have developed rapidly. In the ENEA Frascati Research Center, researchers developed a resonant cavity BCM for pulsed proton medical linacs [8]. Furthermore, the PSI reported the progress of the cavity BCMs used in proton therapy facilities and successfully demonstrated noninvasive beam current measurements in the range 0.1–10 nA with a resolution of 0.05 nA in the energy range 238–70 MeV [9].

This paper presents the design of a dielectric-filled cavity BCM. The working frequency was tuned to 146 MHz to match the second harmonic of the pulse rate. To minimize the cavity size working at such a low frequency, a ceramic plate was inserted into the cavity gap to increase the equivalent capacitance. As a result, the equivalent inductance decreased accordingly to maintain the resonance frequency, which made the cavity compact. Section 2 introduces the theory and basic formulae for the cavity monitor. Section 3 describes the electromagnetic design of the cavity BCM using CST Microwave Studio. In Section 4, we introduce offline tests, including measurements of the working frequency, quality factors, normalized shunt impedance, and linearity and position independence. Section 5 presents an analysis of the effects of proton beams of different energies on the output signal amplitude and beam current sensitivity. In Section 6, we demonstrate demodulation of the induced signal and evaluate the beam current resolution. Finally, we provide a summary and concluding remarks in the final section.

2. Basic theory of BCMs

When a charged beam travels through a cavity, the beam wakefield excites the eigenmodes of the cavity. Each resonant mode has an energy loss because of the finite conductivity of the cavity material and coupling ports, and the quality factor can characterize the performance [10].

2.1. Single-bunch operation mode

The loaded quality factor Q_L characterizes the total energy loss and is defined as

$$Q_L = \frac{\omega U}{P}, \tag{1}$$

where ω is the resonant angular frequency, U is the energy stored in the cavity for a resonant mode, and P is the energy loss per angular oscillation of the mode, which consists of the power dissipation on the inner wall of the cavity caused by the ohmic loss p_{wall} and the loss caused by the coupling ports p_{ext}. The unloaded quality factor Q_0 and external factor Q_{ext} can be used to characterize p_{wall} and p_{ext}, respectively.

The normalized shunt impedance R/Q_0 describes the energy interaction intensity between the charged particle beam and the cavity [11]. If the phase shift between the electric field and the beam is neglected, the ideal normalized shunt impedance is defined as

$$\hat{R}/Q_0 = \frac{\left|\int E(\vec{s})d\vec{s}\right|^2}{\omega U} = \frac{V^2}{\omega U}, \tag{2}$$

where the numerator represents the integration of the electric field in the resonant mode along the beam passage. If a phase shift occurs during the beam transition, the normalized impedance can be represented as

$$R/Q_0 = \frac{\left|\int E\left(\vec{s}\right)\cos\left(\frac{\omega z}{\beta c}\right)d\vec{s}\right|^2}{\omega U} = \hat{R}/Q_0.T^2, \quad (3)$$

where βc represents the particle velocity, and T is the transit time factor, which is a function of the beam velocity. Considering the energy loss at the cavity wall and coupling ports, the decay time constant τ is defined as

$$\tau = \frac{Q_L}{\omega}. \quad (4)$$

This represents the time required for the stored energy to reduce to 1/e of its original value. When the bunch interval is significantly longer than the decay time constant, there is no interference from the energy induced by successive bunches. In this case, the cavity monitor operates in single-bunch mode.

After a longitudinal Gaussian-distributed bunch whose RMS length is σ_z passes through the cavity, the output voltage at the port with characteristic impedance Z can be calculated as follows [12, 13]:

$$\begin{aligned} V &= \frac{q\omega}{2}\sqrt{\frac{Z}{Q_{ext}}(R/Q)}\exp\left(-\frac{\omega^2\sigma_z^2}{2c^2}\right)\exp\left(-\frac{t}{2\tau}\right)\exp\left(i\omega_n t\right) \\ &= V_0\exp\left(-\frac{t}{2\tau}\right)\exp\left(i\omega_n t\right). \end{aligned} \quad (5)$$

In the TM010 (monopole) mode in a cylindrical cavity, the axial electric amplitude near the central axis remains relatively constant [14], making it suitable for measuring the beam current.

2.2. Multiple-bunch operation mode

When the bunch interval is less than or close to the decay time constant, the cavity monitor operates in multiple-bunch modes, and the output voltage is the superposition of each bunch signal. Assuming that the beam interval is T_b and the number of bunches is m, the output voltage of the cavity BCM is given by

$$\begin{aligned} V_m &= V_0\sum_0^{m-1}\exp\left(i\omega_n m T_b\right)\exp\left(-m\frac{T_b}{2\tau}\right) \\ &= V_0\frac{1-\exp\left(i\omega_n m T_b\right)\exp\left(-m\frac{T_b}{2\tau}\right)}{1-\exp\left(i\omega_n T_b\right)\exp\left(-\frac{T_b}{2\tau}\right)}. \end{aligned} \quad (6)$$

To evaluate the effects of different working frequencies on the output signal of the cavity BCM, we define $\omega_n = N\frac{2\pi}{T_b} + \Delta\omega$, where N is an integer. Then,

$$V_m = V_0\frac{1-\exp\left(im\Delta\omega T_b\right)\exp\left(-m\frac{T_b}{2\tau}\right)}{1-\exp\left(i\Delta\omega T_b\right)\exp\left(-\frac{T_b}{2\tau}\right)}. \quad (7)$$

As the number of bunches increases, the output voltage converges to a constant value.

$$V_m = V_0\frac{1}{1-\exp\left(i\Delta\omega T_b\right)\exp\left(-\frac{T_b}{2\tau}\right)}. \quad (8)$$

When $\Delta\omega = 0$, that is, the working frequency of the cavity BCM is an integer multiple of the bunch frequency, the output signal reaches its maximum [14, 15].

$$V_m = V_0\frac{1}{1-\exp\left(-\frac{T_b}{2\tau}\right)} = V_0\frac{1}{1-\exp\left(-\frac{\omega T_b}{2Q_L}\right)}. \quad (9)$$

Compared to the single-bunch operation mode, the multiple-bunch mode can amplify the output signal by the gain factor, which has an obvious advantage in the case of low-intensity measurements. In practice, we can adjust the external quality factor to ensure that the cavity monitor operates in the multiple-bunch mode.

3. Design and simulation

3.1. Cavity geometry

In multiple-bunch mode, a cavity BCM prefers to operate in the frequency harmonics of the beam repetition rate to increase the output signal. The superconducting cyclotron produces Gaussian-shaped proton bunches at a repetition rate of 73 MHz. Gaussian-shaped bunches with a bunch charge q, bunch spacing T, and RMS length σ_z can be expanded using a cosine series with $\omega_0 = \frac{2\pi}{T}$ [16]:

$$I_b\left(t\right) = \frac{q}{t} + \sum_{m=1}^{\infty} I_m\cos\left(m\omega_0 t\right), \quad (10)$$

where

$$I_m = 2\frac{q}{T}\exp\left(-\frac{m^2\omega_0^2\sigma_z^2}{2}\right). \quad (11)$$

It is evident that a lower harmonic contains more beam energy. However, if the cavity operates at the first harmonic frequency, it typically suffers from direct noise from the power generator. In addition, a low working frequency makes the

cavity BCM considerably large. Therefore, the working frequency of the cavity BCM was matched to the second harmonic of the bunch repetition rate. Usually, a pillbox cavity serves as a BCM owing to its simple structure and precise machining [5]. However, when working at a low frequency of 146 MHz in TM010 mode, the pillbox cavity radius is 78.4 cm. Such a large size prevents precise manufacturing and installation of the cavity BCM.

A reentrant cavity was employed to minimize the cavity size, whose resonant characteristics can be analogized by two lumped elements [17, 18]: the capacitor plate (C_{gap}) and cavity wall inductor (L_{wall}). C_{gap} can be calculated as follows:

$$C_{gap} = \frac{\varepsilon_r \varepsilon_0 \pi \left(r_{max}^2 - r_{min}^2\right)}{d}, \tag{12}$$

where ε_r is the relative permittivity of the material filling in the gap, ε_0 is the permittivity of vacuum, d is the gap height, and r_{min} and r_{max} are the outer and inner radii of the capacitor plate, respectively. The cavity wall and inner metal cylinder can be regarded as a coaxial line with closed termination based on transmission line theory. The impedance Z, as seen at the input of the coaxial line, can be calculated as

$$Z = jZ_0 \tan\left(\frac{2\pi h}{\lambda}\right), \tag{13}$$

where Z_0 is the characteristic impedance of the coaxial part, which is determined by the outer and inner radii of the coaxial line, h is the length of the coaxial line, and λ is the free-space wavelength. It is evident that the impedance Z is inductive when the length of the coaxial line is shorter than $\lambda/4$. The cavity resonates when the gap capacitance compensates for the cavity wall inductor, and the resonant frequency is given by

$$\omega_0 = \frac{1}{\sqrt{Z_{wall}.C_{gap}}}. \tag{14}$$

At a working frequency of 146 MHz, $\lambda/4$ was 510 mm, rendering the coaxial length of the reentrant cavity BCM too large to be acceptable. Owing to the limited longitudinal installation space, the cavity length was set to within 150 mm, which led to a decrease in Z_{wall}. C_{gap} must be increased to satisfy the resonance frequency, which can be achieved by decreasing the gap length or filling the gap with dielectric materials. For comparison, a common reentrant cavity and dielectric-filled reentrant cavity with the same working frequency of 146 MHz were designed, as shown in Fig. 2; the detailed dimensions are listed in Table 2.

According to the comparison, inserting a dielectric material can effectively increase the gap length, leading to a longer interaction path between the charged particle and cavity, which amplifies the output signal. Increasing the gap length also reduces the sensitivity of the TM010 mode frequency. The simulation results show that if the gap height of the dielectric-filled reentrant cavity is 16.7 mm, the sensitivity of the working frequency to the gap height decreases from 23 to 3 MHz/mm, which makes fabrication easier. Dielectric materials use Macor ceramic because of its easy and precise machinability [19].

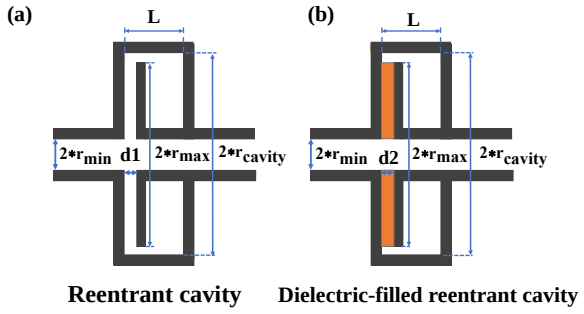

Fig. 2. Outline of a common reentrant cavity (a) and dielectric-filled reentrant cavity (b).

Table 2. Reentrant cavity and dielectric-filled reentrant cavity dimensions (same working frequency of 146 MHz).

Dimensions	Normal cavity	Dielectric-filled cavity
Cavity radius, r_{cavity}	85 mm	85 mm
Cavity length, L	146.7 mm	146.7 mm
Pipe radius, r_{min}	39 mm	39 mm
Plate radius, r_{max}	79 mm	79 mm
Gap length, d	2.65 mm	16.7 mm

3.2. Output signal of BCM

Fig. 3 shows the dielectric-filled reentrant cavity BCM modeled by the CST [20]. The simulation results show that the induced electric and magnetic fields are concentrated in the dielectric plate and coaxial area, validating the lumped-element circuit model, as shown in Fig. 4(a) and (b).

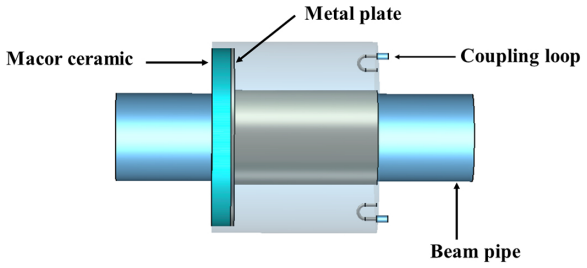

Fig. 3. CST model of the dielectric-filled reentrant cavity.

A higher output signal requires more induced energy inside the BCM for a given external quality factor. Working in multiple-bunch operation modes, the BCM can accumulate more energy from each bunch, making it possible to determine the Q_{ext} flexibly to obtain a reasonable output signal.

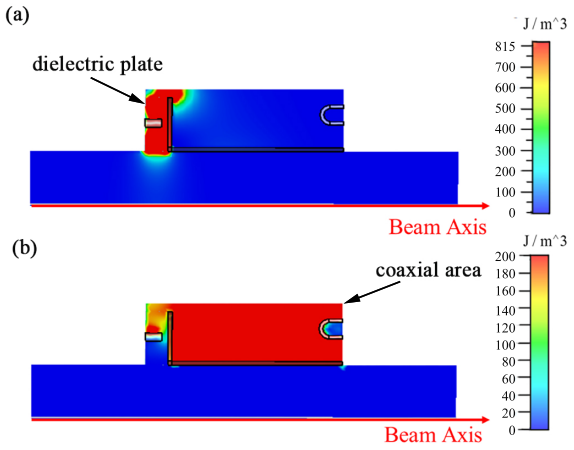

Fig. 4. Energy intensity distribution of the induced electric fields (a) and magnetic fields (b) inside the cavity.

Eq. 9 shows that the detectable signal of the multiple-bunch mode is the product of the gain factor and output signal of the single-bunch mode. An increase in the external quality factor can increase the gain factor. However, this reduces the output signal excited by a single bunch, as illustrated in Fig. 5. Considering that the dielectric loss accelerates the electromagnetic energy decay, the growth of the gain factor is limited. Eventually, the output signal in multiple-bunch mode decreases with an increase in the external quality factor (Fig. 5). Coupling loops were employed to extract the beam current signal, and the port impedance was tuned to 50 Ω. A smaller Qext requires larger coupling loops, which may severely disturb the electromagnetic field distribution inside BCM. Eventually, by adjusting the coupling loop size and orientation in the CST MWS, the external quality factor was optimized to 2000.

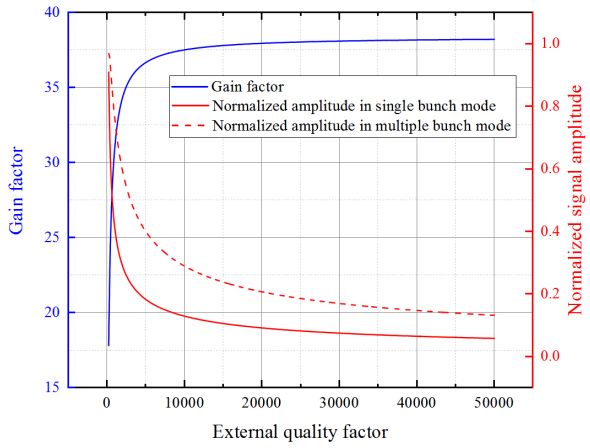

Fig. 5. Effects of the external quality factor on the BCM signal amplitude and gain factor.

In a practical cavity, the resonant frequency may deviate from the design owing to the mechanical tolerance and uncertainty of Macor permittivity. Thus, the output signal will change accordingly, as expressed by Eq. 12. As shown in Fig. 6, the signal amplitude decreased abruptly when the working frequency aways from 146 MHz. To prevent frequency deviation from reducing the output signal, we installed four tuners to adjust the resonant frequency of the cavity. They were placed in the holes of the Macor plates to increase the tuning range.

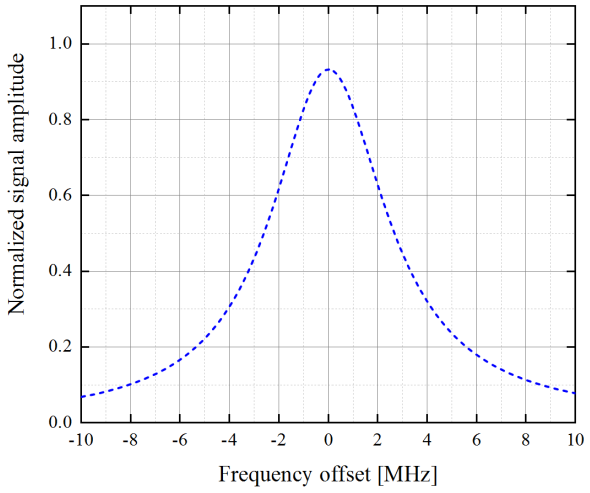

Fig. 6. Effects of frequency offset on the BCM signal amplitude in multiple-bunch mode.

4. Offline tests for prototype cavity

4.1. Manufacture of the prototype cavity

We manufactured the prototype cavity BCM shown in Fig. 7. It comprised three main mechanical components. Part 1 was a beam pipe, Part 2 was a concentric pipe that formed a coaxial line with the beam pipe with a closed termination, and Part 3 was the cavity gap filled with Macor ceramic. The cavity was stainless steel 316L. A 2-mm groove was arranged on a stainless-steel plate to fix the Macor ceramic. The coaxial probes were soldered directly onto the cavity wall. The coupling loops were detachable, which was convenient for tuning the external quality factor. Metal rods were employed as tuners to adjust the resonant frequency, and rulers were installed on the tuners to observe the penetration depth. We did not consider vacuum in the design of the prototype cavity. If the cavity BCM is installed in HUST-PTF, the corrugated pipes will replace the rulers to maintain the vacuum.

4.2. Working frequency and quality factors

Using the vector network analyzer KEYSIGHT E5071C, we obtained the resonant frequency and unloaded and loaded quality factors based on S-parameter measurements [21]. The normalized shunt impedance R/Q_0 was measured using the

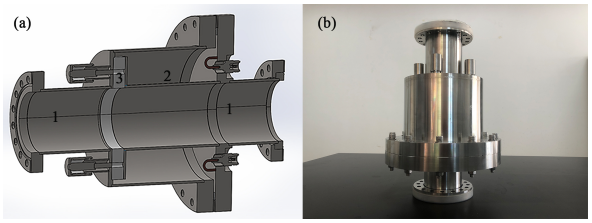

Fig. 7. Mechanical design of the dielectric-filled cavity: (a) cross-section of mechanical design of the cavity BCM; (b) corresponding prototype cavity.

bead-pull method [22]. The measured data agreed well with the simulation results listed in Table 3. Fig. 8 indicates that the tuners could easily adjust the resonant frequency and agree well with the simulation, which proves the correctness of the design. The penetration depth of the tuners could be changed by precession. The moving ranges of the tuners were set from 0 to 15 mm to guarantee sufficient frequency adjustment to satisfy the request. Because the tuners moving inside the cavity exhibited higher tuning sensitivity, the initial position of the tuners was inside the cavity at a depth of 12.5 mm to minimize the tuning sensitivity.

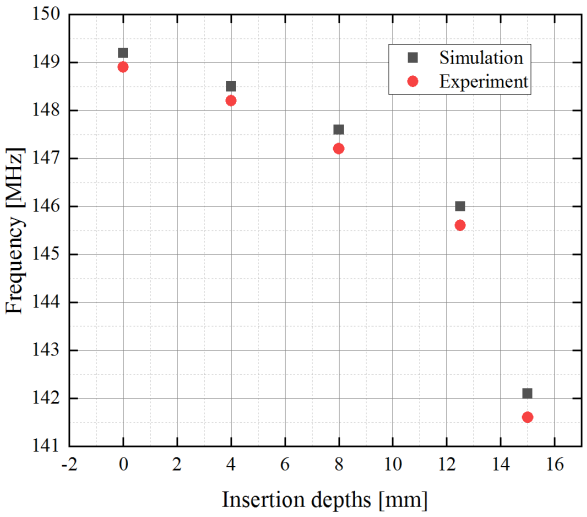

Fig. 8. Insertion depths of the tuners versus the working frequency of the cavity.

4.3. Beam analog measurement

Because HUST-PTF is currently being developed, we can only employ beam analog measurement to characterize the cavity BCM. Stretched-wire measurement is a typical method used to characterize beam monitors. The offline test platform is illustrated in Fig. 9. The prototype cavity was supported by a two-directional displacement platform. A vertical metal wire passing through the center of the cavity served as the longitudinal beam analog. A metal wire was fixed to both sides of the prototype cavity and stretched as tightly as possible. However, the cavity could move transversely with an accuracy of 0.001 mm, precisely simulating an off-axis beam. The 146-MHz sinusoidal signal from a signal generator was fed into the metal wire to excite the electromagnetic fields in the cavity and induce the corresponding voltage signals at the two feedthrough ports. Eventually, the feedthrough ports were connected to an oscilloscope with an FFT function for further analysis. The reliability of the beam analog was confirmed using the CST, in which the input signals of both the metal wire and bunch had the same longitudinal distribution and Gaussian distributions with RMS widths of 1 ns. The output signals in the frequency domain are shown in Fig. 10, which proves the equivalence between the metal wire and the actual bunch.

When a metal wire is employed as a beam analog, the metal wire and beam pipes form a coaxial line, causing electromagnetic energy in the cavity to leak easily through the beam pipe [23]. Therefore, the output signal excited by the metal wire is weaker than that excited by the bunch. For each frequency component, the output amplitudes excited by the metal wire and bunch are linearly correlated, which can be written as

$$V_{bunch} = k.V_{wire}, \tag{15}$$

where K is a constant.

In practice, the proton bunch has a transverse size, and protons at different locations undergo different normalized shunt impedances. A weighted method based on the superposition principle is employed to simulate the bunch with a transverse size [24, 25]. A grid is defined in the cross-sectional plane of the beam, and each grid point represents the transverse position of the metal wire. According to the transverse distribution function of the bunch, the output signal is obtained by summing the signals of different grid points with weight factors. A smaller grid step size indicates a more accurate simulation, but a longer experimental time. In practice, we employed a 10×10 mm grid with a step size of 0.2 mm to approximate a Gaussian distribution with 2 σ of 5 mm [26]. The measurement results in Fig. 11 show satisfactory linearity between the output and excitation signals.

An ideal BCM should be independent of beam position. We evaluated the dependence of the output signal on the beam offset using an offline test platform and analogized the bunch at different transverse positions by shifting the platform. The experimental results showed that the transverse position of the beam had a negligible effect on the output signal (Fig. 12). The relative amplitude change was within 0.1% even with a 10-mm beam offset.

5. Induced signal modeling

Proton beam energies are nonrelativistic, leading to energy-dependent velocity and bunch length, resulting in different output signals from the dielectric-filled cavity BCM even at the same beam current. This must be calibrated to guarantee

Table 3. Simulation and cold test results.

Parameters of interest	Simulation results	Cold test results
Resonant frequency	146 MHz	145.7 MHz
Unloaded quality factor	257	238
External factor	2000	2132
Normalized shunt impedance	36.9 Ω	35.5 Ω

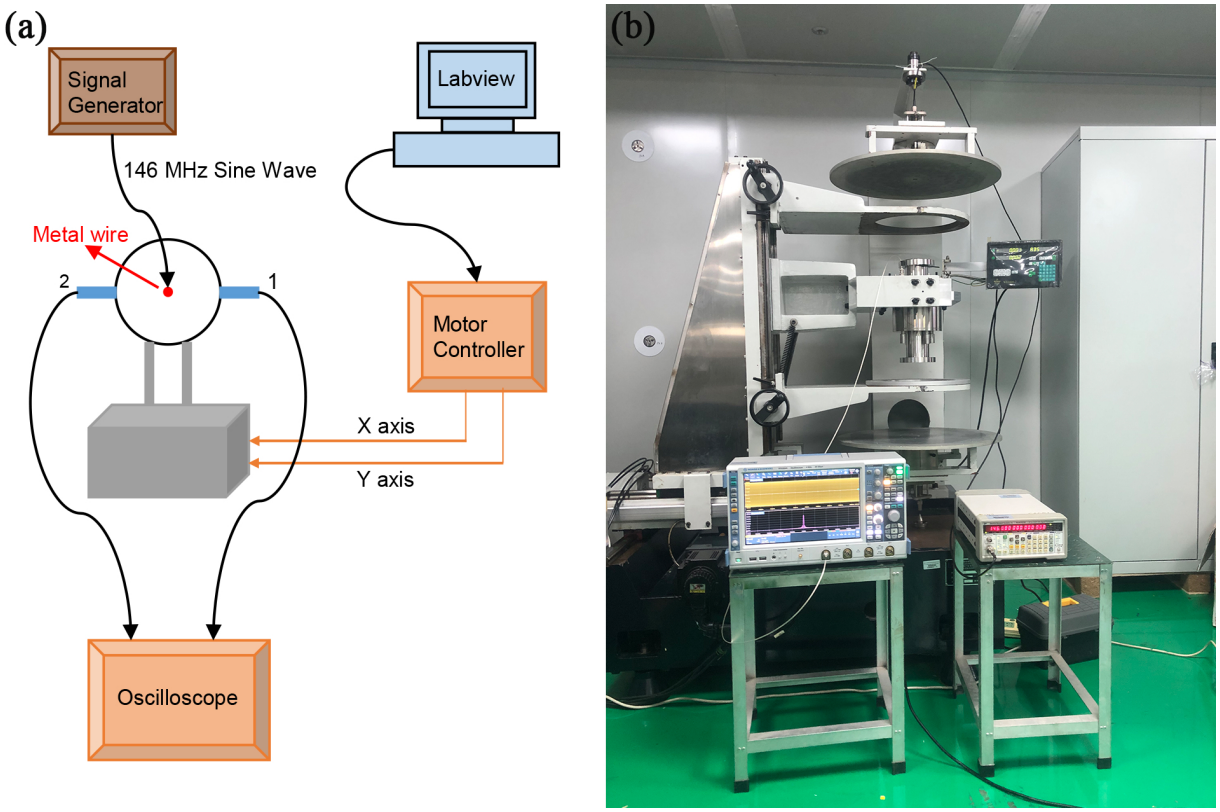

Fig. 9. Layout of the offline test platform. On the left is a schematic of the stretched wire method, and on the right is a photograph of the beam analog measurement.

treatment dose accuracy. The cavity BCM was placed just downstream of the ESS exit such that the bunch could maintain the same approximate length of 200 mm at different proton energies. Five different energies were selected to evaluate the output signals, and the results are listed in Table 4, for which the CST post-processing module calculated the transit time factors. We calculated the output signals at different proton energies according to the cold test results and analytical model in Section 2. The development of the signal envelopes with time is shown in Fig. 13, where we artificially injected proton beam pulses of 7 μs to show a complete process, including signal superposition, a stable peak signal, and signal attenuation. The superconducting cyclotron operated in the CW mode, and the output of the cavity BCM was almost stable if the beam energy remained constant. Eventually, the output signal varied from 66.7 to 997.3 nV when the beam current in the designed range varied from 0.35 to 5 nA. The beam-current sensitivity was 190.6 nV/nA at 70 MeV. Considering that the transit time factor had a minimum value of 70 MeV, the beam current sensitivity was greater than 190.6 nV/nA in most energy cases. In practical operation of the cavity BCM, we must calibrate the output signal of the cavity BCM in every energy case. An ionization chamber will be placed behind the cavity BCM and used as a reference monitor. Considering the increasing momentum spread caused by the degrader, when the location of the cavity BCM changes, it must be recalibrated owing to the increasing bunch length.

6. Demodulation of the output signals

In the case of demodulating the beam current signal, applying a lock-in amplifier has proven to be very successful [27]. Lock-in amplifiers can only extract signals in a defined frequency band and filter out the other frequency components. Because the expected beam current signal is close to the res-

Table 4. Proton beam parameters at the location of the cavity BPM at different energies.

Energy, MeV	Beam current, nA	Transit time factor	Output signal, nV
70	0.35	0.925	66.7
110	1.38	0.949	266.5
150	1.81	0.960	351.6
210	3.41	0.966	664.4
230	5.00	0.972	997.3

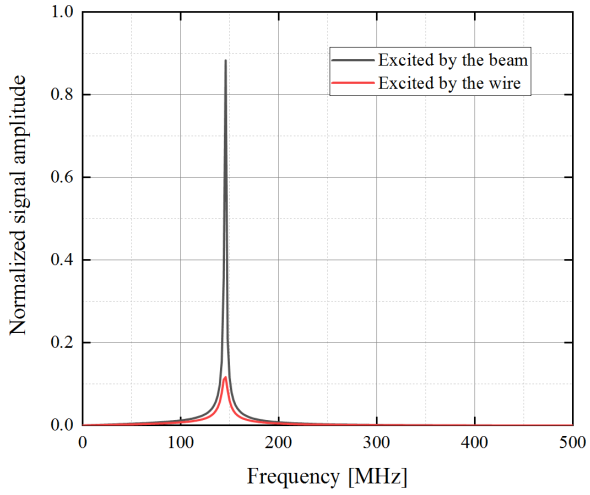

Fig. 10. Comparison of the output signals excited by a bunch and metal wire with the same electric signal.

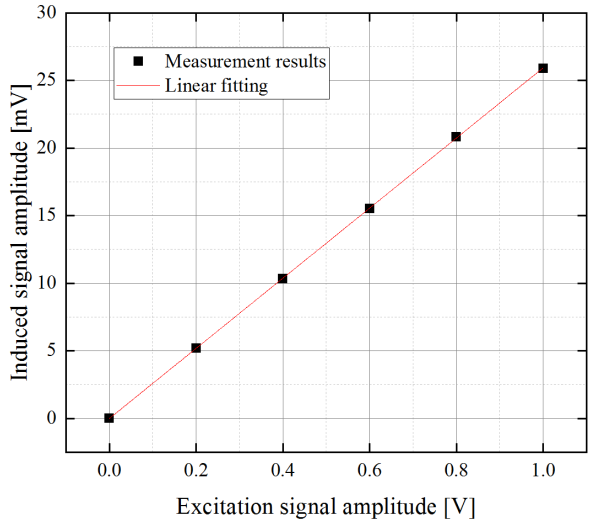

Fig. 11. Induced signal amplitude versus the excitation signal amplitude.

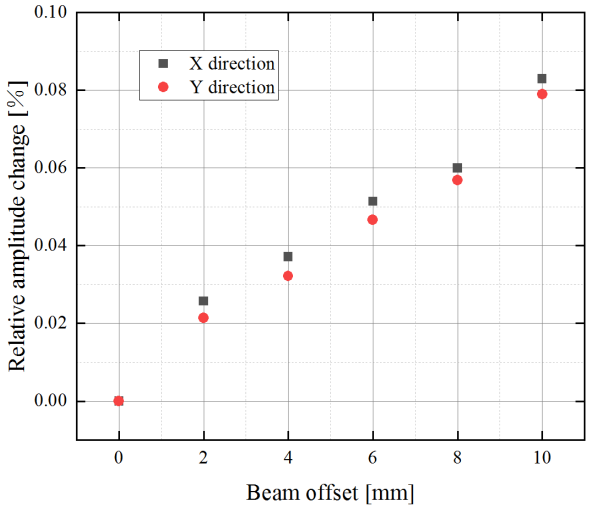

Fig. 12. Relative change in the induced signal amplitude versus beam offset.

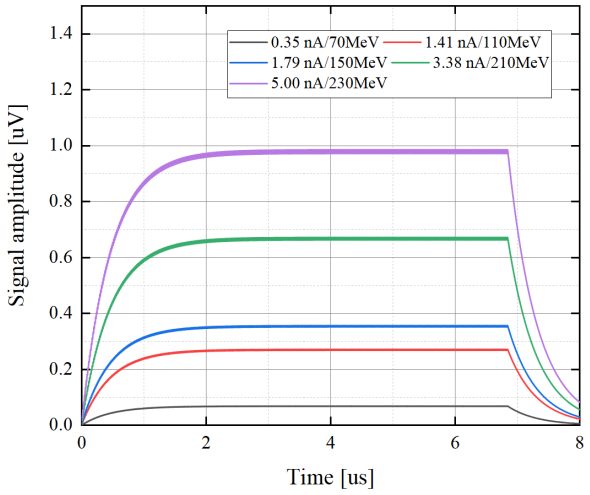

Fig. 13. Output signal envelopes of the cavity BCM in five energy cases.

onant frequency of the fundamental mode, a lock-in amplifier is planned for signal demodulation.

Fig. 14 shows a simplified schematic of a typical lock-in measurement. The weak input signal immersed in noise is split into two channels and separately multiplies with the reference signal with and without a 90°-phase shift. The reference signal is a sine wave with the same frequency as that of the input signal. After passing through low-pass filters, two DC signals with a phase difference of 90° can be obtained. They are fed into analog-to-digital converters, and the amplitude and phase of the input signal can be calculated in the CPU.

The UHFLI Lock-in amplifier (Zurich Instrument AG) covering the frequency range from DC to 600 MHz is planned for use. The arbitrary waveform generator in the UHFLI

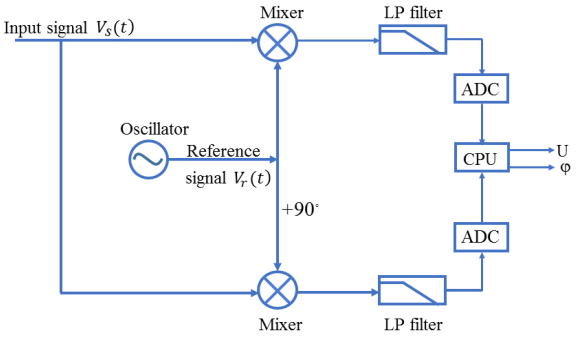

Fig. 14. Schematic of lock-in measurement.

Lock-in amplifier provides a reference signal of 146 MHz. The noise amplitude in the amplifier output port depends primarily on the bandwidth of the LP filter, which corresponds to a time constant. Reducing the filter bandwidth introduces less noise at the expense of the reaction speed; therefore, a good compromise between them must be made. For a 4^{th}- order filter, ten time constants must elapse to obtain an accurate output signal (99%) [28]. We assume that the time constant is set to 50 ms. In this case, the setting time is 0.5 s. According to the user manual, the noise-equivalent power bandwidth is 1.56 Hz.

According to Nyquist's theorem, the amplitude of thermal noise is represented as

$$V_n = \sqrt{4k_B T(K) Z \triangle f}\,(V)\,, \tag{16}$$

where k_B is the Boltzmann Constant, and T(K) is the absolute temperature. Considering an operation temperature of 300 K and a 50 Ω detecting impedance, the thermal noise spectral density is 0.9 $nV/\sqrt{Hz}$. Considering the 4 $nV/\sqrt{Hz}$ equivalent input noise of the UHFLI Lock-in amplifier and the thermal noise, the total noise spectral density at the output port is 4.1 $nV/\sqrt{Hz}$. When the noise-equivalent power bandwidth is 1.56 Hz, the noise voltage at the output port is 5.12 nV.

The calculation results in Section 5 showed that the signal amplitude of the cavity BCM was between 66.7 to 997.3 nV; hence, the signal-to-noise ratio varied from 13.03 to 194.79. Considering that the beam current sensitivity had a minimum value of 190.6 nV/nA at 70 MeV, even in the worst condition (70 MeV, 0.35 nA), the beam current resolution could still reach 0.03 nA, which is a satisfactory result.

7. Conclusion

This paper presents the development of a dielectric-filled reentrant cavity BCM for HUST-PTF. The working frequency of the cavity was designed to be 146 MHz to match the second harmonic of the bunch repetition rate. The CST software was used to optimize both the cavity and pick-up geometries to increase the output signal amplitude. Inserting a dielectric ceramic into the cavity gap can reduce the cavity size and the sensitivity of the working frequency, which reduces the error tolerance and facilitates easier fabrication.

A prototype cavity BCM was fabricated and tested. Based on the S-parameter measurements, the cavity was characterized on a stand-alone test bench. The Q factors and shunt impedances were in good agreement with the simulation results. A stretched wire experiment based on the superposition principle showed that the cavity BCM exhibited satisfactory linearity and position independence. The test results and analytical model demonstrated that the beam current sensitivity was greater than 190.6 nV/nA. A lock-in amplifier is planned to be employed to significantly reduce the noise signal and improve the beam current resolution to 0.03 nA. Although an integration time of 0.5 s limits the functionality of the cavity BCM during patient treatment, it can be used to trigger safety interlocks to handle the beam operation parameters within the expected range. Both analytical and experimental studies have demonstrated that the dielectric-filled cavity BCM is a promising candidate for nondestructive beam current detection at HUST-PTF.

Author Contributions All authors contributed to the study conception and design. Material preparation, data collection, and analyses were performed by Jiqing Li. The mechanical design and experiments were performed by Jiqing Li and Jian Wang. The first draft of the manuscript was written by Jiqing Li, and all authors commented on the previous versions of the manuscript. All authors have read and approved the final manuscript.

8. References

[1] Kayoko Ohnishi, Naoki Nakamura, Hideyuki Harada et al., Proton beam therapy for histologically or clinically diagnosed Stage I non-small cell lung cancer (NSCLC): The first nationwide retrospective study in Japan. Int. J. Radiat. Oncol. Biol. Phys. **106**(1), 82-89 (2020). https://doi.org/10.1016/j.ijrobp.2019.09.013

[2] Zhiyuan Mei, Kuanjun Fan, Zhikai Liang et al., Optimization of a B4C/graphite composite energy degrader and its shielding for a proton therapy facility. Nucl. Instrum. Meth. A **995**, 165127 (2021). https://doi.org/10.1016/j.nima.2021.165127

[3] Shanshan Cao, Yongbin Leng, Renxian Yuan et al., Methods study on high-resolution bunch charge measurement based on cavity monitor. Nucl. Tech. **44**(04), 1–7 (2021). http://doi.org/10.11889/j.0253-3219.2021.hjs.44.040101 **(in**

Chinese)

[4] Belohrad D, Beam charge measurements. In *Proceedings of DIPAC2011* (Hamburg, Germany, 2011), pp. 564-568

[5] Pusch, R. Thorsten, F. Frommberger, W. C. A. Hillert, B. Neff, Measuring the intensity and position of a pA electron beam with resonant cavities. Phys. Rev. ST Accel. Beams. **15**, 112801 (2020). http://doi.org/10.1103/PhysRevSTAB.15.112801

[6] Cao, SS., Yuan, RX., Chen, J et al., Dual-cavity beam arrival time monitor design for the Shanghai soft X-ray FEL facility. NUCL SCI TECH. **30**, 72 (2019). https://doi.org/10.1007/s41365-019-0593-3

[7] J. Chen, S. Cao, Y. Leng et al., Study of the optimal amplitude extraction algorithm for cavity BPM. Nucl. Instrum. Meth. A. **1012**, 165627 (2021). https://doi.org/10.1016/j.nima.2021.165627

[8] P. Nenzi et al., Development of a Passive Cavity Beam Intensity Monitor for Pulsed Proton Beams for Medical Applications. In *Proceedings of IBIC'19* (Malmö, Sweden, 2019), pp. 41-44. http://doi.org/10.18429/JACoW-IBIC2019-MOCO022

[9] Srinivasan S, Duperrex P A, Schippers J M, Beamline Characterization of a Dielectric-filled Reentrant Cavity Resonator as Beam Current Monitor for a Medical Cyclotron Facility. Phys. Med. **78**, 101-108 (2020). http://doi.org/10.1016/j.ejmp.2020.09.006

[10] Shanshan Cao, Yongbin Leng, Renxian Yuan, Jian Chen, Optimization of beam arrival and flight time measurement system based on cavity monitors at the SXFEL. IEEE Transactions on Nuclear Science. **68**, 2–8 (2021). https://doi.org/10.1109/TNS.2020.3034337

[11] Shin S, Wendt M, Design Studies for a High Resolution Cold Cavity Beam Position Monitor. IEEE Transactions on Nuclear Science. **57**, 2159–2166 (2010). http://doi.org/10.1109/TNS.2010.2049503

[12] Walston S, Boogert S, Chung C et al., performance of a high resolution cavity beam position monitor system. Nucl. Instrum. Meth. A. **578**, 1–22 (2007). http://doi.org/10.1016/j.nima.2007.04.162

[13] Forno M D, Craievich P, Baruzzo R et al., A novel electromagnetic design and a new manufacturing process for the cavity BPM (Beam Position Monitor). Nucl. Instrum. Meth. A. **662**, 1–22 (2012). https://doi.org/10.1016/j.nima.2011.09.040

[14] R. Lorenz, Cavity beam position monitors. AIP Conf. Proc. **451**, 53 (1998). http://doi.org/10.1063/1.57039

[15] Whittum D H, Kolomensky Y, Analysis of an asymmetric resonant cavity as a beam monitor. Review of Scientific Instruments. **70**, 2300-2313 (1999). http://doi.org/10.1063/1.1149756

[16] Srinivasan, Sudharsan, Duperrex et al., Dielectric-Filled Reentrant Cavity Resonator as a Low-Intensity Proton Beam Diagnostic. Instruments. **2**, 24-24 (2018). http://doi.org/10.3390/instruments2040024

[17] Srinivasan, Duperrex, Reentrant cavity resonator for low intensity proton beam measurement. In *Proceedings of IPAC2018* (Vancouver, Canada, 2018), pp. 2341–2344. https://doi.org/10.18429/JACoW-IPAC2018-WEPAL069

[18] M Giordano et.al., On the design of a reentrant square cavity as resonator for low-frequency ESR spectroscopy. J. Physics. E Sci.Instrum. **16**, 774-779 (1983). http://doi.org/10.1088/0022-3735/16/8/017

[19] Macor Machinable Glass Ceramic Properties. http://accuratus.com/macormats.html

[20] CST STUDIO SUITE. https://www.cst.com

[21] Chen, J., Leng, YB., Yu, LY. et al. Beam test results of high Q CBPM prototype for SXFEL. NUCL SCI TECH. **28**, 51 (2017). https://doi.org/10.1007/s41365-017-0195-x

[22] Peter A. Mcintosh, Perturbation Measurements on RF Cavities at Daresbury. In *Proceedings of EPAC1994* (Daresbury Laboratory, London, 1994), pp. 1283.

[23] Wang Q, Luo Q, Sun B, Design and performance study of an improved cavity bunch length monitor based on an optimized offline test scheme. Nucl. Instrum. Meth. A. **968**, 163975 (2020). http://doi.org/10.1016/j.nima.2020.163975

[24] S.J. Russell, J.D. Gilpatrick, J.F. Power, R.B. Shurter, Characterization of beam position monitors for measurement of second moment. In *Proceedings of the 1995 Particle Accelerator Conference* (Texas, USA, 1995), pp. 2580–2582. http://doi.org/10.1109/PAC.1995.505624

[25] F.F. Wu, Z.R. Zhou, B.G. Sun et al., Design and Calculation of the stripline beam position monitor for HLS II storage ring. In *Proceedings of IPAC'13* (Shanghai, China, May 2013)

[26] Chen W, Yang J, Qin B et al., Transmission calculation and intensity suppression for a proton therapy system. Nucl. Instrum. Meth. A. **881**, 82-87 (2017). http://doi.org/10.1016/j.nima.2017.10.047

[27] Ursic R, Flood R, Piller C, 1 nA beam position monitoring system. In *Proceedings of the 1997 Particle Accelerator Conference* (Vancouver, Canada, 1997), pp. 2131–2133.

[28] Principles of lock-in detection and the state of the art. https://www.zhinst.cn/china/en/resources/principles-of-lock-in-detection